Ultra-sensitive chemical vapor detection using micro-cavity photothermal spectroscopy

Juejun Hu*

Department of Materials Science & Engineering, University of Delaware, Newark, Delaware 19716, USA
**hujuejun@udel.edu*

Abstract: In this paper, I systematically investigated Micro-Cavity PhotoThermal Spectroscopy (MC-PTS), a novel technique for ultra-sensitive detection of chemical molecular species. I first derive the photothermal enhancement factor and noise characteristics of the technique using a generic theoretical model, followed by numerical analysis of a design example using chalcogenide glass micro-disk cavities. Guidelines for sensor material selection and device design are formulated based on the theoretical insight. The numerical analysis shows that this technique features a record photothermal enhancement factor of 10^4 with respect to conventional cavity-enhanced (multi-pass) infrared absorption spectroscopy, and is capable of detecting non-preconcentrated chemical vapor molecules down to the ppt level with a moderate cavity quality factor of 10^5 and a pump laser power of 0.1 W. Such performance qualifies this technique as one of the most sensitive methods for chemical vapor spectroscopic analysis.

OCIS codes: (140.3948) Micro-cavity devices; (070.5753) Resonators; (130.3120) Integrated optics devices; (130.3060) Infrared; (130.6010) Sensors; (300.6430) Spectroscopy, photothermal; (300.1030) Absorption.

References and links

1. S. E. Bialkowski, "Photothermal Spectroscopy Methods for Chemical Analysis," in *Chemical Analysis: A Series of Monographs on Analytical Chemistry and Its Applications*, J. D. Winefordner, ed. (John Wiley & Sons 1996).
2. A. Sedlacek, and J. Lee, "Photothermal interferometric aerosol absorption spectrometry," Aerosol Sci. Technol. **41**(12), 1089–1101 (2007).
3. N. Dovichi, and J. Harris, "Laser Induced Thermal Lens Effect for Calorimetric Trace Analysis," Anal. Chem. **51**(6), 728–731 (1979).
4. C. C. Davis, and S. J. Petuchowski, "Phase fluctuation optical heterodyne spectroscopy of gases," Appl. Opt. **20**(14), 2539–2554 (1981).
5. H. A. Schuessler, S. H. Chen, Z. Rong, Z. C. Tang, and E. C. Benck, "Cavity-enhanced photothermal spectroscopy: dynamics, sensitivity, and spatial resolution," Appl. Opt. **31**(15), 2669–2677 (1992).
6. H. A. Schuessler, S. H. Chen, Z. C. Tang, and Z. Rong, "Cavity-enhanced photothermal spectroscopy and detection," Appl. Surf. Sci. **48-49**, 254–256 (1991).
7. R. W. Boyd, and J. E. Heebner, "Sensitive disk resonator photonic biosensor," Appl. Opt. **40**(31), 5742–5747 (2001).
8. J. Nadeau, V. Ilchenko, D. Kossokovski, G. Bearman, and L. Maleki, "High-Q whispering-gallery mode sensor in liquids," Proc. SPIE **4629**, 172–180 (2002).
9. G. Farca, S. I. Shopova, and A. T. Rosenberger, "Cavity-enhanced laser absorption spectroscopy using microresonator whispering-gallery modes," Opt. Express **15**(25), 17443–17448 (2007).
10. A. Nitkowski, L. Chen, and M. Lipson, "Cavity-enhanced on-chip absorption spectroscopy using microring resonators," Opt. Express **16**(16), 11930–11936 (2008).
11. B. Koch, Y. Yi, J. Zhang, S. Znameroski, and T. Smith, "Reflection-mode sensing using optical microresonators," Appl. Phys. Lett. **95**(20), 201111 (2009).
12. J. Hu, N. Carlie, L. Petit, A. Agarwal, K. Richardson, and L. C. Kimerling, "Cavity-enhanced infrared absorption in planar chalcogenide glass resonators: experiment & analysis," J. Lightwave Technol. **27**(23), 5240–5245 (2009).
13. B. B. Kyotoku, L. Chen, and M. Lipson, "Sub-nm resolution cavity enhanced microspectrometer," Opt. Express **18**(1), 102–107 (2010).
14. A. M. Armani, R. P. Kulkarni, S. E. Fraser, R. C. Flagan, and K. J. Vahala, "Label-free, single-molecule detection with optical microcavities," Science **317**(5839), 783–787 (2007).

#134476 - $15.00 USD Received 3 Sep 2010; revised 28 Sep 2010; accepted 28 Sep 2010; published 5 Oct 2010

15. J. Homola, S. Yee, and G. Gauglitz, "Surface plasmon resonance sensors: review," Sens. Actuators B Chem. **54**(1-2), 3–15 (1999).
16. J. Hu, S. Lin, L. C. Kimerling, and K. Crozier, "Optical trapping of nanoparticles in resonant cavities," Phys. Rev. A (submitted to).
17. J. Hu, "Planar Chalcogenide Glass Materials and Devices," Massachusetts Institute of Technology Ph.D Thesis (2009).
18. S. Arnold, S. I. Shopova, and S. Holler, "Whispering gallery mode bio-sensor for label-free detection of single molecules: thermo-optic vs. reactive mechanism," Opt. Express **18**(1), 281–287 (2010).
19. *Encyclopedia of Optical Engineering*, R. G. Driggers and C. Hoffman, ed. (CRC Press 2003).
20. A. Rogalski, "Comparison of photon and thermal detector performance," In *Handbook of Infra-red Detection Technologies*, M. Henini and M. Razeghi, ed. (Elsevier Science 2002).
21. J. Homola, "Surface plasmon resonance sensors for detection of chemical and biological species," Chem. Rev. **108**(2), 462–493 (2008).
22. F. Vollmer, D. Braun, A. Libchaber, M. Khoshsima, I. Teraoka, and S. Arnold, "Protein detection by optical shift of a resonant microcavity," Appl. Phys. Lett. **80**(21), 4057–4059 (2002).
23. K. De Vos, J. Girones, T. Claes, Y. De Koninck, S. Popelka, E. Schacht, R. Baets, and P. Bienstman, "Multiplexed antibody detection with an array of silicon-on-insulator microring resonators," IEEE Photonics J. **1**(4), 225–235 (2009).
24. J. Hu, X. Sun, A. Agarwal, and L. C. Kimerling, "Design guidelines for optical resonator biochemical sensors," J. Opt. Soc. Am. B **26**(5), 1032–1041 (2009).
25. P. Lucas, A. Doraiswamy, and E. King, ""Photoinduced structural relaxation in chalcogenide glasses," J. Non-Cryst. Sol. **332**, 35–42 (2003).
26. A. Rogalski, J. Antoszewski, and L. Faraone, "Third-generation infrared photodetector arrays," J. Appl. Phys. **105**(9), 091101 (2009).
27. S. C. H. O. T. T. North America, Inc., "Infrared Chalcogenide Glass IG3," *http://www.us.schott.com/advanced_optics/english/download/ir_grade_ig3_dec09.pdf*
28. J. Hu, N. Carlie, N. N. Feng, L. Petit, A. Agarwal, K. Richardson, and L. C. Kimerling, "Planar waveguide-coupled, high-index-contrast, high-Q resonators in chalcogenide glass for sensing," Opt. Lett. **33**(21), 2500–2502 (2008).
29. J. Hu, N. N. Feng, N. Carlie, L. Petit, A. Agarwal, K. Richardson, and L. C. Kimerling, "Optical loss reduction in high-index-contrast chalcogenide glass waveguides via thermal reflow," Opt. Express **18**(2), 1469–1478 (2010).
30. G. R. Elliott, D. W. Hewak, G. S. Murugan, and J. S. Wilkinson, "Chalcogenide glass microspheres; their production, characterization and potential," Opt. Express **15**(26), 17542–17553 (2007).
31. T. Gensty, and W. Elsasser, "Semiclassical model for the relative intensity noise of intersubband quantum cascade lasers," Opt. Commun. **256**(1-3), 171–183 (2005).
32. S. Shibata, M. Horiguchi, K. Jinguji, S. Mitachi, T. Kanamori, and T. Manabe, "Prediction of loss minima in infrared optical fibers," Electron. Lett. **17**(21), 775 (1981).
33. J. S. Sanghera, V. Q. Nguyen, P. C. Pureza, F. H. Kung, R. Miklos, and I. D. Aggarwal, "Fabrication of Low-Loss IR-Transmitting $Ge_{30}As_{10}Se_{30}Te_{30}$ Glass Fibers," J. Lightwave Technol. **12**(5), 737–741 (1994).
34. T. Ikegami, "Differential Temperature Controller for Stable Temperature Control of a Nonlinear Optical Crystal at Approximately 200 °C," Jpn. J. Appl. Phys. **39**(Part 1, No. 8), 4814–4815 (2000).
35. A. Densmore, M. Vachon, D.-X. Xu, S. Janz, R. Ma, Y.-H. Li, G. Lopinski, A. Delâge, J. Lapointe, C. C. Luebbert, Q. Y. Liu, P. Cheben, and J. H. Schmid, "Silicon photonic wire biosensor array for multiplexed real-time and label-free molecular detection," Opt. Lett. **34**(23), 3598–3600 (2009).

1. Introduction

Perhaps the most widely used spectroscopic technique for chemical vapor analysis, infrared (IR) spectroscopy probes the characteristic vibration spectra of molecular species, and provides a wealth of structural and chemical information. In conventional direct absorbance measurement, the presence of chemical molecules leads to infrared absorption at the fingerprint wavelength regions, which is then detected as reduction of transmitted or reflected optical signal. Despite its simplicity, such direct absorption measurement, however, is highly susceptible to noise caused by scatterers (e.g. aerosol, suspended particulates and even air turbulence) for field-based (i.e., deployed, outside the laboratory) applications. Scattering and reflection due to these scatterers can significantly interfere with the measurement and lead to false positive alarms.

To overcome the limitations of conventional direct absorbance measurement, indirect IR spectroscopic techniques have been implemented. Among them, PhotoThermal Spectroscopy (PTS) has been recognized as a highly sensitive and precise method for measuring infrared molecular absorption. Since optical scattering/reflection does not generate a photothermal signal, PTS is particularly suitable for field applications where scattering is often a major concern [1]. For example, PTS has been successfully applied to aerosol absorption

#134476 - $15.00 USD Received 3 Sep 2010; revised 28 Sep 2010; accepted 28 Sep 2010; published 5 Oct 2010

measurement where optical scattering almost completely overshadows optical absorption [2]. In addition to its immunity to scattering interference, the measured optical signal can be amplified by photothermal effects in PTS. Such amplification is quantified using an enhancement factor, defined as the ratio of optical signal magnitudes caused by photothermal effects and by direct absorption [3]. Enhancement factors up to ~2000 with respect to conventional transmission-based IR spectroscopy have been experimentally demonstrated, making PTS a highly sensitive technique for trace chemical analysis [4].

The sensitivity of the PTS technique can be further improved by introduction of optical resonant cavity enhancement. Improved PTS sensitivity has been demonstrated by placing the sample to be analyzed inside a Fabry-Perot etalon optical cavity. When the optically absorbing sample is irradiated by a pump laser beam, the etalon resonance modification due to thermo-optic effects is detected as the photothermal signal [5, 6]. In this paper, I will examine a new Micro-Cavity PhotoThermal Spectroscopy (MC-PTS) technique, where the conventional etalon cavity consisting of bulk mirror assembly is substituted by a micro-cavity such as microsphere, micro-ring or micro-disk. An important advantage of the MC-PTS technique over conventional cavity-enhanced PTS using Fabry-Perot cavities is its inherently superior sensitivity: in conventional cavity-enhanced PTS, the pump laser spot and hence the photothermal interaction volume is typically much smaller than the cavity mode volume; therefore, the photothermal effect becomes spatially localized and a large fraction of the cavity volume remains 'cold' and is not utilized. In contrast, in the case of MC-PTS, both the pump and probe light can be tuned to resonate inside the micro-cavity and maximize their optical mode spatial overlap. As a consequence of such a doubly-resonant configuration, both the optical absorption process of the pump beam and the thermal amplification enhancement factor are maximized, which in turn leads to very high absorption detection sensitivity. Moreover, whereas the photothermal enhancement factor of conventional PTS techniques is limited by the optical and thermal properties of sample materials, the thermal properties of micro-cavities used in MC-PTS can be engineered through material and geometry design to achieve record large photothermal enhancement factors, as I will illustrate in the design example section. Additional benefits of using a micro-cavity include short response time due to its small thermal mass (which also helps to reduce 1/f noise by using high frequency chopped measurement), device miniaturization, elimination of complicated alignment, reduced ambient turbulence by micro-environment control, and the possibility of planar integration with other photonic or electronic components. While micro-cavities have been explored by several groups worldwide for cavity-enhanced spectroscopy [7-13], application of micro-cavities for MC-PTS has been scarce until a recent experimental demonstration for protein molecule detection [14]. Further, a general study of the MC-PTS technique is still lacking.

This paper aims at filling the gap by introducing a systematic theoretical analysis on the MC-PTS technique. This paper is organized as follows: the general properties of the MC-PTS technique are first derived using a generic micro-cavity model. The photothermal enhancement factor and noise contributions from different mechanisms are analyzed to predict the limit of detection (LOD) of the technique. The theoretical insight is then applied to develop an optimization strategy of material and device design for MC-PTS. Following the generic analysis, I numerically examine a design example using chalcogenide glass micro-disk cavities. The example shows that by proper selection of material and cavity designs, dramatic LOD improvement over conventional cavity-enhanced infrared absorption spectroscopy can be achieved.

2. Generic model of an MC-PTS device

2.1 Operating principle of an MC-PTS device

The generic pump-probe configuration of an MC-PTS device is illustrated in Fig. 1. The core component of the device is an optical micro-cavity, which in the most general case can either be a traveling wave cavity such as micro-ring, micro-disk or micro-sphere, or a standing wave

#134476 - $15.00 USD Received 3 Sep 2010; revised 28 Sep 2010; accepted 28 Sep 2010; published 5 Oct 2010

cavity such as a multi-layer Bragg cavity or a point defect in a photonic crystal slab. The cavity is thermally connected to a heat sink (e.g. the substrate on which the micro-cavity device is fabricated) through a thermal conductance G. Given its large thermal mass, the heat sink may be regarded to be held at a constant temperature T_0, which will be used as a reference point for the temperature rise in the micro-cavity. In the pump-probe configuration, a high-power pump beam is actively locked to one of the resonant frequencies of the cavity through a feedback loop which monitors the transmitted intensity in real-time, and is used to induce optical absorption and photothermal effects in the cavity. When optically absorbing molecules are present in the ambient surrounding the cavity, the optical resonant mode of the pump beam interacts with these molecular species evanescently: such interaction converts optical energy of the pump beam into heat via optical absorption. Consequently, the temperature of the cavity will increase from T_0 to T_0 + dT when thermal equilibrium is established between the photothermal heat generation and heat dissipation through the thermal conductance. The resulting temperature change dT translates to a cavity resonant wavelength change $d\lambda_p$ due to thermo-optic effect:

$$d\lambda_p = \kappa \cdot dT \tag{1}$$

where κ is the thermo-optic coefficient of the micro-cavity (the subscript p following λ denotes that the wavelength λ_p is associated with the probe beam). Such a resonant wavelength shift is then detected by a low-power probe beam using wavelength or intensity interrogation [15]. The basic operating principle of MC-PTS is summarized in Fig. 2.

One advantage of using such a pump-probe configuration lies in the inherent flexibility of probe wavelength selection. The probe light measures the resonant frequency shift due to thermo-optic refractive index modification of the cavity material; notably, such index variation can be measured at a wavelength different from the pump wavelength, provided that the resonant cavity is designed to support optical resonance at both wavelengths. Therefore, one could take advantage of mature low cost, high performance laser and detector components for the probe beam by choosing a probe wavelength in visible or near-infrared.

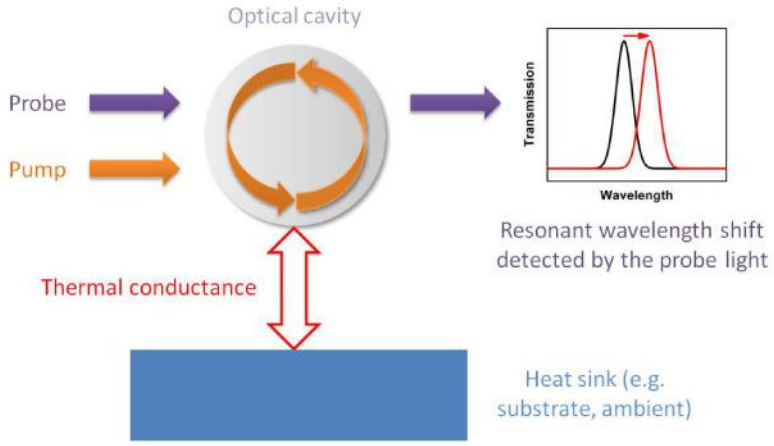

Fig. 1. Illustration of the generic configuration of a micro-cavity device for MC-PTS.

#134476 - $15.00 USD Received 3 Sep 2010; revised 28 Sep 2010; accepted 28 Sep 2010; published 5 Oct 2010

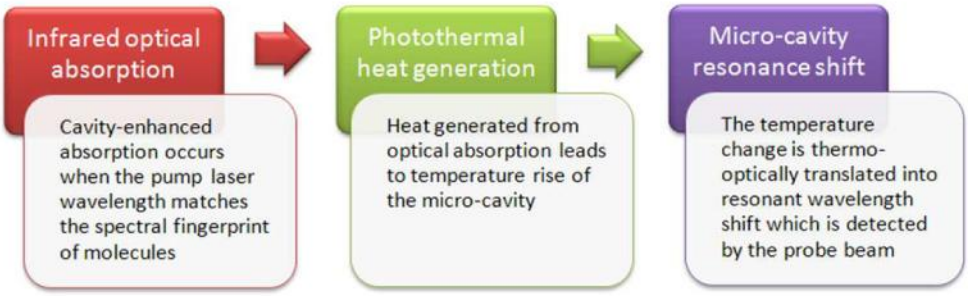

Fig. 2. Flow of the micro-cavity photothermal detection process

2.2 Photothermal signal and enhancement factor

Without losing generality, I assume the micro-cavity has a loaded quality factor Q and is critically coupled to the pump beam, i.e. the fraction of pump light entering the cavity is unity. The total optical energy stored in the cavity at steady state is then given by [16]:

$$W = \frac{\varepsilon_0}{2}\int_c \varepsilon_c |E_0|^2 \, dV = \frac{QP}{2\omega}\int_c \varepsilon_c |E_N|^2 \, dV \tag{2}$$

where ε_c gives the spatial dielectric constant distribution of the cavity, E_0 is the electric field complex amplitude of the cavity mode, P is the pump light power coupled into the cavity, ω is the angular frequency of pump light, and the field E_N is the dimensionless eigenmode of the micro-cavity, normalized so that $\int_c |E_N|^2 \, dV = 1$. The integrals are carried out across the entire cavity, as is denoted by the subscript c. Denote the optical absorption coefficient of the vapor surrounding the cavity as α and according to standard cavity perturbation theory, the decay time constant of optical energy in the cavity due to molecular absorption may be written as:

$$t_d = \frac{2}{c_0 n \alpha} \cdot \frac{\int_c \varepsilon_c |E_N|^2 \, dV}{\int_e |E_N|^2 \, dV} \tag{3}$$

and the optical energy loss rate (which is equal to the photothermal heat generation rate) in the cavity is given by:

$$P_c = \frac{W}{t_d} = \frac{QP\lambda n\alpha}{8\pi} \cdot \int_e |E_N|^2 \, dV \tag{4}$$

Here c_0 is the velocity of light in vacuum, n is the index of refraction (real part) of the sensing medium surrounding the cavity, λ represents the pump wavelength, and the subscript e in the integrals specifies that the integration domain covers only the evanescent wave in the surrounding medium. When the dynamic equilibrium of photothermal heat generation and heat dissipation through the thermal conductance to the heat sink is reached, the temperature change dT of the cavity is given by:

$$dT = \frac{P_c}{G} = \frac{QP\lambda n\alpha}{8\pi G} \cdot \int_e |E_N|^2 \, dV \tag{5}$$

where G is the thermal conductance which has a dimension of power divided by temperature. Equation (5) gives the photothermal signal dT as a result of molecular absorption. The photothermal resonant wavelength shift $d\lambda_p$ may also be derived by combining Eq. (1) and Eq. (5). The photothermal enhancement factor E for the pump-probe configuration can be

#134476 - $15.00 USD Received 3 Sep 2010; revised 28 Sep 2010; accepted 28 Sep 2010; published 5 Oct 2010

defined as the ratio of the fractional transmitted power change of the probe beam dI_p to the fractional transmitted power change of the pump beam dI, since the former is induced by the photothermal effect whereas the latter is the direct consequence of optical absorption. If I assume that the cavity quality factor Q is the same at both pump and probe wavelengths, maximum photothermal enhancement factor is achieved when the following conditions are met: 1) the cavity also operates near the critical coupling regime at the probe wavelength; and 2) $d\lambda_p << \lambda_p/Q$. In this case, the fractional power change of the probe beam dI_p transmitted through the cavity can then be given by multiplying $d\lambda_p$ by the maximum slope of the critically-coupled cavity transmission curve:

$$dI_p = \frac{3\sqrt{3}}{4\lambda_p} Q \cdot d\lambda_p = \frac{3\sqrt{3}}{32} \cdot \frac{\lambda n \alpha \kappa}{\lambda_p \pi G} \cdot \int_e |E_N|^2 \, dV \cdot PQ^2 \tag{6}$$

On the other hand, optical absorbance experienced by the pump beam in the limit of $d\lambda_p << \lambda_p/Q$ is given by [17]:

$$dI \sim \frac{\alpha\lambda}{n_c \pi} \cdot Q \tag{7}$$

Here n_c denotes refractive index of the cavity material. Note that the Q-factor in Eq. (7) represents the contribution of absorption enhancement effect in conventional multi-pass absorption spectroscopy. The enhancement factor E is given by the ratio of dI_p to dI:

$$E = \frac{3\sqrt{3}}{32} \cdot \frac{n_c n \kappa}{\lambda_p G} \cdot \int_e |E_N|^2 \, dV \cdot PQ = \frac{3\sqrt{3}}{32} \cdot \frac{\Gamma n_c n \kappa}{\lambda_p G} \cdot PQ \tag{8}$$

where $\Gamma = \int_e |E_N|^2 \, dV$ can be considered as the fractional cavity modal confinement in the surrounding medium where the target molecular species is present.

The linear dependence of optical absorbance dI on Q is a consequence of resonantly enhanced optical path length in the cavity. In contrast, the photothermal signal dI_p becomes quadratically dependent on Q. The contribution of cavity enhancement effect to the photothermal signal dI_p is two-fold: the optical absorption of the pump and hence photothermal heat generation is enhanced roughly by a factor of Q; and the resonant peak width is inversely proportional to Q such that even a small resonant wavelength shift $d\lambda_p$ translates to a large probe intensity change dI_p which is increased by a factor of Q (the first equality in Eq. (6), leading to another factor of Q boost of dI_p. Equation (8) suggests that the enhancement factor is proportional to the cavity Q-factor. This is also consistent with previous analysis by other authors [14, 18]. Therefore, we can expect very large photothermal enhancement with respect to conventional cavity-enhanced absorption spectroscopy by using a high-Q micro-cavity for MC-PTS.

2.3 Frequency dependence of photothermal signal

Equation (6) and Eq. (8) provide the photothermal signal at steady state. In most practical application scenarios, however, chopped measurement is employed to suppress noise at unwanted frequencies (e.g. 1/f noise at low frequencies) and hence to improve Signal-to-Noise Ratio (SNR). Therefore, it is important to understand the frequency dependence of the photothermal signal in MC-PTS. Photothermal signal frequency dependence may be derived by solving the heat flow equation with a sinusoidal input of heat flux. The photothermal enhancement factor of a micro-cavity with a heat capacity C measured using a sinusoidal input at a frequency f is given by:

$$E(f) = \frac{E(0)}{\sqrt{1+4\pi^2 f^2 \tau^2}} = \frac{3\sqrt{3}}{32} \cdot \frac{\Gamma n_c n \kappa}{\lambda_p G \sqrt{1+4\pi^2 f^2 \tau^2}} \cdot PQ \tag{9}$$

#134476 - $15.00 USD Received 3 Sep 2010; revised 28 Sep 2010; accepted 28 Sep 2010; published 5 Oct 2010

where $\tau = C/G$ is the thermal time constant of the micro-cavity.

2.4 Noise analysis

To determine the limit of detection of the technique, it is necessary to evaluate both the photothermal signal dT as well as the noise sources in the measurement. Since MC-PTS relies on thermo-optic effect for signal transduction, there are mainly two sources of noise: thermal noise and read-out noise. The former includes: 1) temperature fluctuation (TF) noise due to statistical spontaneous temperature fluctuation of the cavity; 2) absorption fluctuation (AF) noise originating from temperature variation in the micro-cavity caused by in-coupled laser power fluctuation; and 3) heat sink (HS) thermal noise resulting from the temperature fluctuations of the heat sink. The read-out (RO) noise mainly refers to errors associated with accurate determination of the resonant wavelength position. Finally, 1/f noise may add to the overall noise as well. The origin of 1/f noise, however, is still an issue of debate and often warrants a case-by-case inspection. Practically, 1/f noise can be suppressed by adopting a high frequency chopped measurement. For these reasons 1/f noise will not be covered in this paper. The total noise is the sum of all the noise contributions:

$$\langle \delta T \rangle = \sqrt{\langle \delta T_{TF} \rangle^2 + \langle \delta T_{AF} \rangle^2 + \langle \delta T_{HS} \rangle^2 + \langle \delta T_{RO} \rangle^2 + \langle \delta T_{1/f} \rangle^2} \tag{10}$$

2.4.1 Temperature fluctuation noise

For a micro-cavity with a heat capacity C at thermal equilibrium, the magnitude of the temperature fluctuation noise can be derived from the fluctuation-dissipation theorem as [19]:

$$\langle \delta T_{TF} \rangle = \sqrt{\frac{k_B T_0^2}{C}} \tag{11}$$

and the power spectral density of root mean square temperature fluctuation noise is:

$$\langle \delta T_{TF}(f) \rangle = \frac{2T_0\sqrt{k_B B}}{\sqrt{G(1+4\pi^2 f^2 \tau^2)}} \tag{12}$$

where T_0 is micro-cavity temperature, k_B represents the Boltzmann constant and B denotes the measurement bandwidth. Since the sensor needs to operate in a sensing medium (typically air) rather than vacuum, the dominant heat transfer mechanism is most likely to be thermal conduction rather than radiation. Therefore I exclude radiative contribution to the factor G and hence background fluctuation noise here [20].

It is also worth noting that the temperature fluctuation noise and the photothermal signal exhibit identical frequency response. As a result, temperature fluctuation noise simply cannot be reduced by changing chopping frequency in detection.

2.4.2 Absorption fluctuation noise

When optical absorption is present in the cavity, laser power fluctuation translates to temperature change of the micro-cavity. In the limit of very dilute vapor, optical absorption in the cavity mainly arises from intrinsic cavity material absorption and background absorption from the sensing medium. Analogous to Eq. (4), power spectral density of this noise mechanism $\langle \delta T_{AF}(f) \rangle$ is directly correlated to the laser intensity noise by:

$$\langle \delta T_{AF}(f) \rangle = \frac{Q\lambda}{8\pi G}(n\Gamma\alpha_{bg} + n_c\alpha_c) \cdot \langle \delta P(f) \rangle \tag{13}$$

in which α_{bg} gives the background absorption from the sensing medium, α_c denotes the micro-cavity material absorption coefficient, and $\langle \delta P(f) \rangle$ is the power spectral density function of

#134476 - $15.00 USD Received 3 Sep 2010; revised 28 Sep 2010; accepted 28 Sep 2010; published 5 Oct 2010

pump laser intensity noise (only considering the laser power coupled into the cavity). We should also note that although scattering (e.g. scattering from roughness or material density non-uniformity) is often one of the major loss sources limiting the cavity Q-factor, it does not contribute to this noise mechanism.

2.4.3 Heat sink thermal noise

In the previous analysis, the heat sink (e.g. the substrate on which the device is fabricated) is assumed to be held at a constant temperature T_0. However, the heat sink temperature is subjected to variations in practice due to ambient temperature variation or residual noise from the temperature stabilization loop. Since the micro-cavity and the heat sink are thermally connected through the thermal conductance G, heat sink temperature fluctuation also translates to micro-cavity temperature change. Since the micro-cavity resonant wavelength is determined by the micro-cavity temperature rather than the temperature difference between the micro-cavity and the heat sink, it is expected that the heat sink temperature fluctuation will add to sensor noise. Power spectral density of this noise contribution can be derived by solving the heat flow equation in the frequency domain and the results give:

$$\left\langle \delta T_{HS}(f) \right\rangle = \frac{\left\langle \delta T_0(f) \right\rangle}{\sqrt{1+4\pi^2 f^2 \tau^2}} \tag{14}$$

where $\left\langle \delta T_0(f) \right\rangle$ is the power spectral density function of the heat sink temperature fluctuation.

2.4.4 Read-out noise

According to Eq. (1), measurement of the photothermal effect induced by trace chemicals requires accurate determination of the resonant wavelength λ_p. The issue of resonant wavelength measurement has been investigated in several different contexts, in particular label-free bio-sensing using Surface Plasmon Resonance (SPR)[21] and dielectric resonators [22, 23]. There are typically three interrogation schemes for bio-sensing applications: angular, wavelength, and intensity interrogation. While angular interrogation is often difficult to implement for micro-cavity sensors, the latter two interrogation schemes may be applied for MC-PTS.

Intensity interrogation looks at the intensity modulation caused by photothermal resonant wavelength shift. Note that the enhancement factor analysis in section 2.2 is based on intensity interrogation. The read-out noise superimposed on $d\lambda_p$ is linked to the coupled pump beam power fluctuation by dividing the fractional power change of the probe beam $\left\langle \delta P_p(f) \right\rangle / P_p$ with the maximum slope of the cavity transmission curve:

$$\left\langle \delta \lambda_p(f) \right\rangle = \frac{4\sqrt{3}\lambda_p}{9Q} \cdot \left\langle \delta P_p(f) \right\rangle / P_p \tag{15}$$

Note that the subscript ‘p’ denotes quantities associated with the probe beam, as read-out noise originates from probe beam power fluctuations and is thus independent of the pump beam properties. Equivalently the read-out noise may be expressed in terms of cavity temperature fluctuation:

$$\left\langle \delta T_{RO}(f) \right\rangle = \frac{4\sqrt{3}\lambda_p}{9Q\kappa} \cdot \left\langle \delta P_p(f) \right\rangle / P_p \tag{16}$$

The other contribution to read-out noise is frequency noise associated with the probe laser. Such noise may be suppressed by using frequency stabilization strategies such as the Pound-Drever-Hall (PDH) technique to well below the thermal noise limit and is thus not further discussed in this paper.

#134476 - $15.00 USD Received 3 Sep 2010; revised 28 Sep 2010; accepted 28 Sep 2010; published 5 Oct 2010

In wavelength interrogation, transmission spectra of the micro-cavity are repeatedly measured across its resonant peak to determine the in situ time evolution of resonant wavelength. Based on the figure-of-merit time-normalized sensitivity S* and a peak fitting algorithm, we have recently developed a systematic method to evaluate read-out noise in wavelength interrogated sensors [24]. The details of read-out noise analysis in wavelength interrogation are more involved and therefore will not be covered in this paper.

3. Material selection and device optimization for MC-PTS

Understanding the signal enhancement and noise characteristics of MC-PTS provides valuable insights for material and device design. The ultimate goal of optimization is to improve signal enhancement while suppressing noise. Other factors that need to be taken into account include detection specificity and device robustness.

3.1 Material down-selection

Based on the discussions above, the following set of material selection criteria can be formulated:

1) Infrared optical transparency

Since the characteristic spectral absorption features of most chemical and biological species are located in the mid- to far-IR wavelength range (2 to 25 μm), the constituent materials of the micro-cavity need to be transparent at these wavelengths to enable full spectrum fitting and target species identification. Therefore, the selection favors materials consisting of heavy elements to reduce phonon absorption in the infrared. Further, to minimize excess free carrier absorption, dielectric materials and wide-bandgap semiconductors are preferred over narrow-gap semiconductors. Examples of IR-transparent materials include chalcogenides, halides, heavy metal oxides, and certain compound semiconductors (e.g. ZnSe).

2) Low thermal conductivity

3) Process compatibility with low optical loss device fabrication

4) High thermo-optic coefficient

Equation (8) suggests that the photothermal enhancement factor is maximal in a thermally isolated (small thermal conductance G), high-Q cavity with high thermo-optic coefficient.

5) Long-term chemical, structural, and thermal stability in the operating environment

This requirement excludes the so-called “fragile” glasses with a mean coordination number < 2.4, as these glasses typically feature relatively low glass transition temperature (T_g) and are susceptible to sub-T_g structural relaxation [25].

3.2 Device optimization

To maximize photothermal signal, the micro-cavity should be thermally isolated from the heat sink. For on-chip device designs, micro-fabricated suspended structures employed in infrared bolometers have been proven to be highly effective in minimizing thermal leakage to the substrate, and thermal conductance in the order of 10^{-8} W/K has been demonstrated [26]. The same design concept may be implemented for MC-PTS as well. Some possible design variations include pedestal structures and thin film devices suspended on an insulating membrane.

We can also see from Eq. (8) and the noise analysis that neither the cavity size nor its mode volume explicitly enters the formulae of photothermal enhancement factor and noise sources. Therefore, the device figure-of-merit for improving MC-PTS sensor detection limit is the cavity Q-factor rather than finesse.

Lastly, even though the proposed MC-PTS sensing mechanism can operate in both gaseous and aqueous environment, it is ideally suited for vapor detection given the much

#134476 - $15.00 USD Received 3 Sep 2010; revised 28 Sep 2010; accepted 28 Sep 2010; published 5 Oct 2010

lower thermal conductivity of air (0.024 W/mK) as compared to that of liquid water (0.6 W/mK). In addition, the strong infrared optical absorption of water also prohibits most infrared spectroscopic applications.

4. A design example: pedestal chalcogenide glass micro-disk resonator for ultra-sensitive chemical vapor detection using MC-PTS

4.1 Material selection

To In this section, I will illustrate an MC-PTS device design example using pedestal micro-disk resonator made of IG3 chalcogenide glass ($Ge_{30}As_{13}Se_{32}Te_{25}$)[27]. The rationales for this material selection include the wide infrared transparency, low thermal conductivity, and high thermo-optic coefficient of this glass composition. The relevant thermal and optical properties of the IG3 glass are listed in Table 1. On the device processing front, we have previously demonstrated that chalcogenide glasses can be fabricated into planar high-Q micro-disk resonators by combining CMOS backend compatible lift-off patterning and post-fabrication thermal reflow treatment [28, 29], thereby opening up the prospect for high volume manufacturing.

Table 1. Key thermal and optical properties of IG3 infrared chalcogenide glass [27]

IR optical transparency window	1.2 to 12 μm
Refractive index	2.80 @ 4.0 μm
Thermal conductivity	0.22 W/mK
Specific heat	1.55 J/cm^{3}K
Thermo-optic coefficient dn/dT	1.3×10^{-4} K^{-1}

4.2 Device design

Figures 3a and 3b show schematic diagrams of the proposed chalcogenide glass micro-cavity device for MC-PTS applications. The device consists of a micro-disk cavity (resonator) made of IG3 glass, a pedestal which mechanically supports the suspended micro-disk cavity, and a planar bus waveguide on the substrate to evanescently couple the pump and probe beams into the cavity. In the following analysis, I assume both pump and probe wavelengths to be around 4 μm, the overhang length to be 10 μm (Fig. 3b), and the micro-disk thickness and diameter to be 1 μm and 100 μm, respectively.

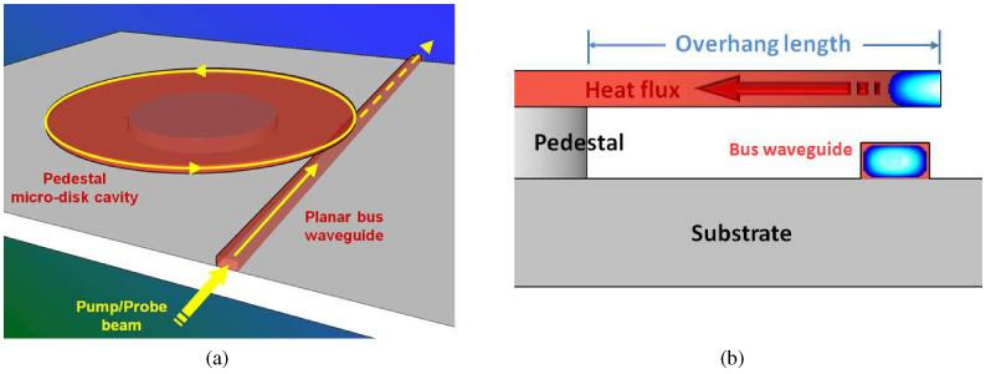

Fig. 3. (a) Schematic tilted view of an on-chip pedestal micro-disk cavity made of chalcogenide glass for MC-PTS applications; (b) cross-section of the pedestal micro-disk cavity (not to scale).

To solve for the effective thermal conductance G, I notice that the thermal conductivity of IG3 glass is almost an order of magnitude larger than that of air. It is assumed that the substrate and the pedestal have large thermal conductivity so that they are considered to be held at a constant temperature T_0 all the time. In the case that the two paths are comparable in

#134476 - $15.00 USD Received 3 Sep 2010; revised 28 Sep 2010; accepted 28 Sep 2010; published 5 Oct 2010

their thermal conductance magnitude, I can make the approximation that the overall thermal conductance is the direct sum of two parts: the thermal conductance through the glass micro-disk and through the surrounding air:

$$G = G_{disk} + G_{air} \tag{17}$$

The two thermal conductance components may be separately calculated by mapping the thermal diffusion problem into a cross-section (Fig. 3b) in a cylindrical coordinate and numerically solving the 2-d Laplace equation. Using an air thermal conductivity value of 0.024 W/mK and the IG3 glass thermal conductivity listed in Table 1, the numerical solution gives a total effective thermal conductance of G = 2.8 × 10^{-5} W/K. If I further neglect the temperature variation across the WGM mode profile, the average steady-state temperature rise (photothermal signal) is given by:

$$dT = \frac{P_c}{G} = \frac{\Gamma \alpha \lambda}{\pi n_g G} \cdot PQ \tag{18}$$

Substituting Eq. (18) into Eq. (9) yields the photothermal enhancement factor at steady state (f = 0):

$$E(0) = \frac{3\sqrt{3}}{4} \cdot \frac{\Gamma \kappa}{\lambda_p G} \cdot PQ = PQ \cdot 0.48(W^{-1}) \tag{19}$$

The time constant of the photothermal signal is τ = C/G ~4 × 10^{-5} s, corresponding to a nearly flat sensor response up to measurement frequencies of ~10 kHz. Equation (19) suggests that even for a moderate cavity Q-factor [17, 30] of 2 × 10^5 and a pump laser power of 100 mW, a photothermal enhancement factor as large as 10^4 is expected with respect to direct cavity-enhanced (multi-pass) infrared absorbance measurement.

4.3 Noise analysis

As for the noise, since the measurement bandwidth is usually much smaller compared to the chopping frequency, the noise amplitude may be well approximated by a constant over the measurement bandwidth. In this case the measured noise amplitude becomes proportional to the square root of the bandwidth $\sqrt{B}$. Thus here I look at bandwidth normalized temperature noise amplitudes, which are given by Eq. (12), Eq. (13) and Eq. (16) as:

$$\frac{\langle \delta T_{TF}(f) \rangle}{\sqrt{B}} = \frac{2T_0\sqrt{k_B}}{\sqrt{G(1+4\pi^2 f^2 \tau^2)}} = 2.6\times10^{-7} K \cdot Hz^{-\frac{1}{2}} \tag{20}$$

$$\frac{\langle \delta T_{AF}(f) \rangle}{\sqrt{B}} = \frac{Q\lambda n_c \alpha_c}{8\pi G} \cdot \frac{\langle \delta P(f) \rangle}{\sqrt{B}} = 2.3\times10^{-7} K \cdot Hz^{-\frac{1}{2}} \tag{21}$$

$$\frac{\langle \delta T_{RO}(f) \rangle}{\sqrt{B}} = \frac{4\sqrt{3}\lambda_p}{9Q\kappa} \cdot \frac{\langle \delta P_p(f) \rangle}{P_p\sqrt{B}} = 3.3\times10^{-9} K \cdot Hz^{-\frac{1}{2}} \tag{22}$$

Here, intensity noise figures of mid-IR quantum cascade lasers calculated using a semi-classical model are taken as the noise characteristics of the pump and probe sources [31], which give a Relative Intensity Noise (RIN) value of −170 dB/Hz for the 100 mW pump beam and RIN = −150 dB/Hz for the low power probe beam. The measurement chopping frequency is chosen to be 5 kHz, and the heat sink temperature is fixed at 300 K. Since material absorption of chalcogenide glass has both theoretically and experimentally been established to be very low the mid-IR wavelength range [32, 33], I use α_c = 0.1 dB/m as an estimate in Eq. (21). I also neglect background absorption in Eq. (21), as it can be minimized

#134476 - $15.00 USD Received 3 Sep 2010; revised 28 Sep 2010; accepted 28 Sep 2010; published 5 Oct 2010

by carefully selecting the operating wavelength to avoid absorption bands, or by constantly purging the measurement chamber with inert gas. A cavity Q-factor of 2×10^5 is assumed to obtain the listed numbers.

To estimate the heat sink thermal noise, I first use the Wiener-Khintchine theorem to correlate the power spectral density function $\langle \delta T_0(f) \rangle$ to the RMS amplitude of heat sink temperature fluctuation $\langle \delta T_0 \rangle$:

$$\langle \delta T_0 \rangle^2 = \int_0^\infty \left| \langle \delta T_0(f) \rangle \right|^2 df \tag{23}$$

The detailed from of $\langle \delta T_0(f) \rangle$ is instrument-dependent and is often unknown. For simplicity, it is assumed that $\langle \delta T_0(f) \rangle$ is a constant up to a cut-off frequency $\overline{f}$ and vanishes at frequencies above $\overline{f}$. Now Eq. (23) becomes:

$$\langle \delta T_0(f) \rangle = \frac{\langle \delta T_0 \rangle}{\sqrt{\overline{f}}} \tag{24}$$

As a conservative estimate, $\overline{f}$ is taken to be the measurement chopping frequency 5 kHz. In this case, a heat sink RMS temperature fluctuation amplitude of 1 mK (note that sub-mK temperature control has been achieved by several authors[34]) corresponds to:

$$\frac{\langle \delta T_{HS}(f) \rangle}{\sqrt{B}} = \frac{\langle \delta T_0 \rangle}{\sqrt{B\overline{f}(1+4\pi^2 f^2 \tau^2)}} = 8.8 \times 10^{-6} K \cdot Hz^{-\frac{1}{2}} \tag{25}$$

Clearly, heat sink thermal noise is more than one order of magnitude larger than the other noise sources given the assumed conditions. However, I would like to emphasize that this noise does not present a fundamental limit to the MC-PTS technique: in practice it may be partially circumvented by selecting a chopping frequency where $\langle \delta T_0(f) \rangle$ is minimal, or by using a reference micro-cavity to cancel out the temperature fluctuation effect[35].

4.4 Chemical detection sensitivity

Lastly, let's estimate the MC-PTS sensor limit of detection in terms of analyte concentration, a figure which is most commonly used in the sensing community. Assuming a measurement bandwidth window of 1 Hz, Eq. (9) and Eq. (25) yield an absorption detection limit of 2×10^{-9} cm^{-1}, primarily limited by the heat sink thermal noise. Therefore, for a pure analyte gas with an infrared absorption coefficient of 50 cm^{-1} (a typical value for chemical vapors at room temperature and one atmosphere pressure), the concentration detection limit of the proposed MC-PTS device is ~40 ppt (parts-per-trillion). We note that no pre-concentration is yet assumed in deriving this LOD number; thus orders of magnitude further improvement is expected when the MC-PTS technique is coupled with gas pre-concentration schemes, which will bring the LOD well into the sub-ppt range.

5. Conclusion

In this paper, I systematically investigated micro-cavity photothermal spectroscopy as a novel technique for ultra-sensitive detection of chemical species. The doubly-resonant pump-probe configuration leads to efficient, resonantly enhanced infrared absorption as well as superior spectroscopic resolution, and gives rise to record large photothermal enhancement factors exceeding 10^4. Quantitative numerical analysis performed based on a chalcogenide glass micro-cavity sensor design yields an absorption detection limit down to 2×10^{-9} cm^{-1} for a cavity with a moderate quality factor of 2×10^5 and at a pump laser power of 0.1 W, which

#134476 - $15.00 USD Received 3 Sep 2010; revised 28 Sep 2010; accepted 28 Sep 2010; published 5 Oct 2010

corresponds to ~40 ppt chemical vapor molecular detection limit without pre-concentration. Since heat sink temperature fluctuation has been identified as the primary noise source in detection, the analysis also suggests further sensor performance improvement by selecting a measurement chopping frequency where the noise spectral density is minimal, or by using a reference cavity to cancel out the temperature fluctuation effect.

Acknowledgements

The author would like to thank Dr. Xiaochen Sun and Vivek Singh for their helpful comments to the manuscript. The author gratefully acknowledges start-up funding support from the University of Delaware.

#134476 - $15.00 USD Received 3 Sep 2010; revised 28 Sep 2010; accepted 28 Sep 2010; published 5 Oct 2010